Probabilistically Validated Constitutive Model of the Annulus Fibrosus

Sarah K Shaffer[1], Lance Frazer[1], Jack Seifert[2], Brian Stemper[2], Dan Nicolella[1], Timothy Bentley[3]
[1]Southwest Research Institute, San Antonio, TX; [2]Medical College of Wisconsin, Milwaukee, WI; [3] Office of Naval Research, Arlington, VA
sarah.shaffer@swri.org

Disclosures: No conflicts of interest to report.

INTRODUCTION: Lower back and spinal pain is often reported by military pilots and can lead to functional incapacitation [1]. Pilots undergo extreme variations in spinal loading as the aircraft accelerates and decelerates for different maneuvers and flight environments [1]. Probabilistic computational models are one way to assess how flight loading conditions and natural variations in tissue properties might lead to spinal tissue degradation and/or pain. However, for these modeling techniques to be successful, detail must be given to the nonlinear viscoelastic nature of biological tissues that faithfully represent the response at multiple strain magnitudes. The reactive viscoelasticity framework in FEBio provides the capability for modeling biological tissues that meet the stated criteria where the viscoelastic contribution of the material is modeled as weak bonds that break and reform in a stress-free state, and the elastic contribution of the material is modeled with strong bonds [2-3]. As such, the aim of this study is to develop a novel model of the annulus fibrosus (AF), using the reactive-viscoelastic framework, that represents the response of the tissue through a broad range of strains and during repetitive loading.

METHODS: A nonlinear reactive-viscoelastic constitutive model for the annulus fibrosus (AF) was developed, calibrated, and probabilistically validated in FEBio. The AF is composed of concentric layers of collagenous and elastin fibers embedded in a matrix [4]. So, the AF constitutive model was defined as a three-component mixture consisting of a ground matrix (Holmes-Mow) with two reactive-viscoelastic tensile fibers representing collagen and elastin. Both fiber families had an orientation of ±25° (fiber-exp-linear fiber type) and were governed by the same Malkin relaxation function [2,3,5-7]. This nonlinear viscoelastic material model requires 21 material parameters (Table 1; 3 for ground matrix, 8 per fiber, 2 relaxation constants). However, the ground matrix (E = 0.1, v =0.1, beta = 0.8) and first relaxation constant were fixed. The remaining 17 material parameters required to define the constitutive model were identified via optimization using experimental data from 7 AF specimens. Then, a probabilistic analysis was performed to validate the constitutive model using experimental data from a different set of 7 AF specimens. The data was previously collected from porcine AF specimens tested under following protocol: a step-strain procedure (20-minute strain-holds at 4%, 8%, 12%, and 16% engineering strain), followed by a recovery period, and 400 cycles of cyclic loading at 20% ultimate tensile strain at 5 cycles/second (Figure 1) [8]. For parameter identification, sample geometry was simulated in FEBio using 8-node trilinear hexahedral elements and experimental displacements were used to drive the model and predict force. A global optimization scheme was used to identify material parameter values that minimize the normalized squared error (NSE) between the simulated (F_{sim}) and experimental force (F_{exp}) measured at 13 time-points (($NSE = (F_{exp}(t) – F_{sim}(t))^2 / F_{exp}(t)$); Figure 1); optimization was performed with DAKOTA [9]. Material parameter distributions were fitted to a lognormal distribution; this prevented negative material parameters from being selected during the probabilistic validation. For model validation, a probabilistic simulation was performed using Latin Hypercube Sampling (LHS) with each material parameter assigned as a random variable [10]. The fitted lognormal distributions were supplied to DAKOTA's LHS routine to select 170 parameter sets. Then, an FEBio simulation, built from one of the AF samples not used for parameter identification, was performed 170 times (1 simulation for each of the 170 parameter sets). The Wasserstein distance (WD) between the cumulative distribution of experimental data (n = 7) and simulated data (n = 170 simulations) was determined for the 13 timepoints used for parameter identification (Figure 2). As a validation metric, a low WD indicates good agreement between simulation and experimental distributions [11]. The percentage of simulations with predicted force values within 2 standard deviations of the average experimental force was also determined for each timepoint.

RESULTS SECTION: The WD calculated for each of the 13 time-points was between 0.5 and 6.8 N (Table 1). On average, WD in the incremental step strain region (timepoints 1- 8) was 3.2 ± 2.3 N and in the cyclic loading region (timepoints 9-13) was 4.2 ± 0.38 N. At all examined timepoints, 51-90% of the simulations predicted force values within ±2 standard deviations of the mean experimental force.

DISCUSSION: Good agreement was observed between a probabilistic simulation and experimental data for a novel nonlinear viscoelastic material model of the annulus fibrosus. During calibration, the model consistently underestimated peak forces in the strain-hold region but had good agreement within the cyclic loading (Figure 1). This resulted in a wider-range of the validation metric (Wasserstein-distance) to be found in the strain-hold region compared to the cyclic loading portion of the experimental data. To improve model performance in the future, it is likely necessary to include the correlation matrix for model parameters. The main limitation of this study is the small number of samples used to calibrate (n = 7) and validate (n = 7) the material model.

SIGNIFICANCE/CLINICAL RELEVANCE: This work has produced a tissue-level validated nonlinear viscoelastic material model for the annulus fibrosus that could be used within a probabilistic spinal model. This model will be improved in the near-term to include fatigue properties (using the same reactive framework in FEBio), such that long-duration flight mechanics can be better understood in the context of tissue damage development at sub-maximal loads.

REFERENCES: [1] Mastalerz, A., et al., (2022): DOI: 10.3390/ijerph192013413**.** [2] G. Ateshian. 2015, DOI: 10.1016/j.jbiomech.2015.02.019. [3] Ateshian, et. al. (2023). DOI: 10.1115/1.4054983 [4] Yu., et. al., (2007). DOI: 10.1111/j.1469-7580.2007.00707.x [5] Nims, R., et. al. (2017). DOI: 10.1007/s10659-017-9630-9 [6] Fiber-Exp-Linear, FEBio User Manual version 3.6, 2022. [7] Malkin Relaxation Function, FEBio User Manual version 3.6, 2022. [8] Seifert, J., Stemper, B. 2023. Unpublished Data from Medical College of Wisconsin. [9] Efficient Global Optimization, DAKOTA Version 6.15 Theory Manual (2021). [10] Sampling Methods, DAKOTA Version 6.15 Theory Manual (2021). [11] Villani C., 2009. DOI: 10.1007/978-3-540-71050-9_6

ACKNOWLEDGEMENTS: This work was funded by the Office of Naval Research.

IMAGES AND TABLES:

Table 1: The material parameters required for annulus fibrosus constitutive model. The 8 Elastic and Bond parameters were determined separately for both fibers.

Parameter	Description (Unit)	Optimization Range	Solution Range
C_3 Elastic	Exponential stress coefficient (MPa)	(0.01,3)	(0.18, 2.83)
C_4 Elastic	Fiber uncrimping coefficient (unitless)	(0.1, 3)	(0.22, 2.52)
C_5 Elastic	Modulus Straightened Fibers (MPa)	(0.1, 50)	(1.02, 41.68)
λ Elastic	Fiber stretch when straightened(unitless)	(1.01, 1.3)	(1.05, 1.25)
C_3 Bond	Exponential stress coefficient (MPa)	(0.01,3)	(0.18, 2.94)
C_4 Bond	Fiber uncrimping coefficient (unitless)	(0.1, 3)	(0.15, 2.95)
C_5 Bond	Modulus Straightened Fibers (MPa)	(0.1, 50)	(1.02, 49.08)
λ Bond	Fiber stretch when straightened(unitless)	(1.01, 1.3)	(1.12, 1.3)
τ_1	1st characteristic relaxation time (s)	Fixed: 0.01	Fixed: 0.01
τ_2	2nd characteristic relaxation time (s)	(100,1000)	(140, 350)

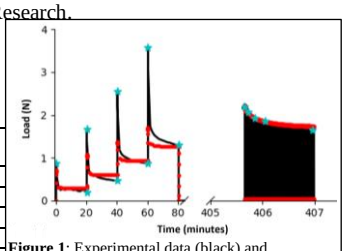

Figure 1: Experimental data (black) and simulation (red) for an AF specimen tested under strain-hold and cyclic loading protocol; the strain-hold response is shown on the left and cyclic loading on the right. Stars (*) indicate 13 timepoints where the optimization sought to minimize normalized squared error.

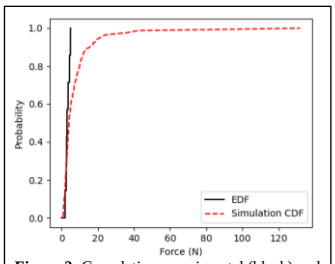

Figure 2: Cumulative experimental (black) and simulation (red dashed) distribution for the peak force seen at the first cyclic pull. The Wasserstein-distance compares the distributions.